J. Fluid Mech. (1976), *vol.* 77, *part* 1, *pp.* 105–128
Printed in Great Britain

A numerical model of the air flow above water waves

By P. R. GENT AND P. A. TAYLOR
Department of Oceanography, University of Southampton, England

(Received 18 July 1975 and in revised form 22 December 1975)

A numerical model is proposed for the flow in a deep turbulent boundary layer over water waves. The momentum equations are closed by the use of an isotropic eddy viscosity and the turbulent energy equation. For small amplitudes the results are similar to those of Townsend's (1972) linear model, but nonlinear effects become important as the ratio of wave height to wavelength increases. With uniform surface roughness z_0, the predicted fractional rate of energy input per radian advance in phase, ζ, decreases slightly with increasing amplitude and is of the same order of magnitude as in Miles' (1957, 1959) and Townsend's linear theories. If z_0 is allowed to vary with position along the wave, however, the fractional rate of energy input can be significantly increased for small amplitude waves. If the variation in z_0 is half the mean value and the maximum wave slope ak is 0·01, we find $\zeta \approx 60\,(\rho_{\mathrm{air}}/\rho_{\mathrm{water}})\,(u_0/c)^2$, where u_0 is the friction velocity and c the wave phase speed. Comparison is also made with recent laboratory and field data.

1. Introduction

The theories of wind wave generation due to Miles (1957, 1959), Benjamin (1959) and others, based on linearization in terms of the maximum wave slope ak, predict a rate of energy input that gives wave growth rates which are approximately an order of magnitude less than those found in the early field studies of Snyder & Cox (1966) and Barnett & Wilkerson (1967). This dichotomy was not resolved by Dobson (1971), whose direct measurements of energy input to the waves gave a wave growth rate similar to the previous sea studies, or by the new turbulent, but still linear, theories of Townsend (1972) and Long (1971), which gave energy input rates similar to the earlier laminar and inviscid theories. More recently several other studies have been made, both in the sea, by Elliott (1972), Hasselmann *et al.* (1973) and Snyder (1974), and in the laboratory, by Shemdin (1969). They all give rates of energy input which are very much closer to the theoretical predictions. The JONSWAP studies (Hasselmann *et al.*) confirm that nonlinear wave interactions can be primarily responsible for wave growth at wavenumbers less than that corresponding to the peak in the energy spectrum. This additional wave growth mechanism clearly confuses our interpretation of observed rates of wave growth at a particular wavenumber, and direct measurements of energy input from the wind are to be preferred for comparisons with our present model.

It is hoped that the nonlinear numerical computations of flow over waves to be presented here may help to indicate the importance of nonlinear effects and predict theoretically the rates of energy input for much larger amplitude waves than was possible before. It should be remarked, however, that our theory applies to the steady flow of air above an infinite train of monochromatic two-dimensional waves. Should nonlinear effects be important the application to wind wave generation by flow above a random sea can only be qualitative. In addition to considering nonlinear effects our numerical model enables us to consider the result of allowing the surface roughness to vary along the wave. This roughness variation could be caused by the presence of much smaller gravity and capillary waves riding on the dominant wave. These are generated by a nonlinear transfer of energy from the dominant wave, and are steepest just forward of the wave crest; see Longuet-Higgins (1969*a*). We might then reasonably expect the maximum roughness to occur at about $\frac{1}{4}\pi$ forward of the crest. It is of interest to note that these smaller waves have recently been observed in the laboratory to be carried along at the phase speed of the dominant wave and thus do not satisfy the dispersion relation. The direct generation of small gravity and capillary waves by the wind (which has recently been studied by Larson & Wright 1975) is not included in the present model. Our numerical experiments with z_0 varying along the wave predict a considerable increase in the rate of energy input to the waves, especially for small amplitude.

For a more thorough review of wind wave generation and associated topics, the reader is referred to the recent review by Barnett & Kenyon (1975).

2. Hypotheses and the equations of motion

The problem considered is that of steady two-dimensional flow in a deep turbulent boundary layer above water waves. The waves are assumed to be periodic in x with wavelength L and, initially, to have a uniform surface roughness z_0. The flow is driven by a horizontal kinematic shear stress u_0^2 applied at the top of the model above the region affected by the waviness of the surface. We work in a frame of reference moving with the waves. The shape of the waves is given by the parametric form

$$z_b = -a\cos k\xi, \quad x = \xi + a\sin k\xi, \tag{2.1}$$

where $k = 2\pi/L$. This results from the conformal mapping used to transform x, z space into a rectangle in ξ, η space, namely

$$\phi = \psi - ia\exp[ik\psi], \tag{2.2}$$

where $\phi = x + iz$ and $\psi = \xi + i\eta$ with the wave surface given by $\eta = 0$. We preferred this to the mapping used by Benjamin (1959) because, in our case, as the amplitude a increases the wave crests become shorter and steeper. We can expand (2.1) to give

$$z_b = -a\cos kx + \tfrac{1}{2}a^2k(\cos 2kx - 1) + O(a^3k^2), \tag{2.3}$$

so that to second order the wave form agrees with that of Stokes waves (see Lamb 1932, art. 250). Sea waves, however, do tend to be even sharper crested and

smoother troughed. The Jacobian of the transformation (2.2) is defined by

$$J = \partial(\xi,\eta)/\partial(x,z) = |d\phi/d\psi|^{-2}, \tag{2.4}$$

and the inviscid incompressible equations of motion may be written as

$$UU_\xi + WU_\eta - (2J)^{-1}(J_\eta UW - J_\xi W^2) = -p_\xi, \tag{2.5}$$

$$UW_\xi + WW_\eta - (2J)^{-1}(J_\xi UW - J_\eta U^2) = -p_\eta \tag{2.6}$$

and

$$(J^{-\frac{1}{2}}U)_\xi + (J^{-\frac{1}{2}}W)_\eta = 0. \tag{2.7}$$

Here U and W are velocities parallel to the ξ,η co-ordinate system. The flow variables can be separated into their mean and turbulent fluctuating parts by putting $U = \bar{U} + u'$, etc. The equations are then ensemble averaged and the system closed by relating the Reynolds stresses to other flow variables. We use turbulent closure hypotheses which are similar but not identical to those of Townsend's (1972) linear theory in preference, for the present, to more complex, higher-order closure schemes. The particular system used is based on the isotropic eddy viscosity model described by Hinze (1959, p. 21), which takes the form

$$-\overline{u_i'u_j'} + \tfrac{2}{3}\bar{E}\delta_{ij} = Ke_{ij}. \tag{2.8}$$

Here e_{ij} is the rate-of-strain tensor $(=(\partial u_i/\partial x_j)+(\partial u_j/\partial x_i)$, in Cartesian co-ordinates) and

$$\bar{E} = \frac{1}{2}\sum_{i=1}^{3}\overline{u_i'^2}$$

is the mean turbulent kinetic energy per unit mass. Our eddy viscosity K is defined by

$$K = (\lambda\bar{E})^{\frac{1}{2}}l, \tag{2.9}$$

where $1/\lambda$ is the equilibrium value of $\bar{E}/u_0^2$. This form for K involves the local value of $\bar{E}$ and so the turbulent energy equation must be added to our system of equations. The mixing length l is given by

$$l = \kappa\left[(\eta+z_0)(1-\exp(-k\eta)) + \left(\int_0^\eta J^{-\frac{1}{2}}d\eta + z_0\right)\exp(-k\eta)\right], \tag{2.10}$$

where κ is von Kármán's constant (taken equal to 0·4). Thus l is proportional to $s+z_0$, where

$$s = \int_0^\eta J^{-\frac{1}{2}}d\eta$$

is the normal distance from the wave when η is small, but is proportional to the distance from the mean surface when η is large (see Townsend 1972). For two-dimensional flow we find from (2.8) that $e_{12} = e_{23} = e_{22} = 0$. Thus the component $\overline{v'^2}$ of the turbulent energy in the cross-flow direction is always $\frac{2}{3}\bar{E}$. The Reynolds stresses are given in curvilinear co-ordinates by

$$\left.\begin{aligned} \tau = -\overline{u'w'} &= K[(J^{\frac{1}{2}}\bar{U})_\eta + (J^{\frac{1}{2}}\bar{W})_\xi], \\ -\overline{u'^2} + \tfrac{2}{3}\bar{E} = \overline{w'^2} - \tfrac{2}{3}\bar{E} &= K[(J^{\frac{1}{2}}\bar{U})_\xi - (J^{\frac{1}{2}}\bar{W})_\eta]. \end{aligned}\right\} \tag{2.11}$$

In place of the above hypothesis Townsend assumed the Reynolds stresses to be fixed proportions of the turbulent kinetic energy and commented against the use of an isotropic model. Our reason for using the isotropic model is basically that we wanted the shear stress τ to include the second term on the right-hand side of (2.11). This can be important, when the wave amplitude is large, in places

where the first term of the right-hand side of (2.11) is small. Use of this form for τ without the expressions for the diagonal elements of (2.11) inevitably leads to computational instability owing, in effect, to a negative horizontal diffusion of $\overline{U}$. A disadvantage of the isotropic model is that it gives a value of $\overline{u'^2}/\overline{w'^2}$ which varies near unity whereas atmospheric observations over land (Busch 1973) suggest a a value of three. A closure hypothesis which avoids this contradiction by considering stresses in a frame of reference orientated parallel and perpendicular to the local flow direction might be possible. It would, however, involve considerable additional complication which we felt was not worthwhile. Taylor, Gent & Keen (1976) compare results over a fixed wavy boundary with both the isotropic model used here and a boundary-layer style of approximation in which the last term in the bracket of the expression for τ in (2.11) is ignored and a fixed partition of turbulent energy is assumed. They found that the results of the latter model were insensitive to the precise partition of turbulent energy and showed that differences between surface values predicted by the two models were small. The justification for use of the isotropic model is admittedly pragmatic and rather weak on physical justification. We think it worth emphasizing, however, that our results will be relatively insensitive to the detailed nature of these closure hypotheses, provided that any length scale introduced is equal to $\kappa(s+z_0)$ near the surface. This view is supported by Reynolds & Hussain (1972), who decided to use an eddy viscosity model but then found the results were "not substantially different" whether it was a constant or a prescribed function of height, but contrasts with the approach of Davis (1972), who found considerable variation between the results obtained with four different, and rather speculative turbulence models. Our aim here is not to investigate new turbulence closure methods but to apply a variant of the traditional closure for turbulent boundary layers to a new flow situation. This type of experiment can, we believe, aid in understanding the overall physics of the flow while comparisons with experimental or field data may in turn help in improving the basic closure hypotheses assumed.

The equations to be solved numerically in conservation form can be written as follows.

Momentum:

$$\begin{aligned}(\overline{U}^2)_\xi + (\overline{U}\overline{W})_\eta + \overline{p}^*_\xi - \frac{J_\eta}{J}\overline{U}\overline{W} + \frac{J_\xi}{2J}(\overline{W}^2 - \overline{U}^2) \\ = K[(J^{\frac{1}{2}}\overline{U})_{\xi\xi} + (J^{\frac{1}{2}}\overline{U})_{\eta\eta}] + [(J^{\frac{1}{2}}\overline{U})_\xi - (J^{\frac{1}{2}}\overline{W})_\eta]\left[K_\xi - \frac{KJ_\xi}{J}\right] \\ + [(J^{\frac{1}{2}}\overline{U})_\eta + (J^{\frac{1}{2}}\overline{W})_\xi]\left[K_\eta - \frac{KJ_\eta}{J}\right] \quad (2.12)\end{aligned}$$

and

$$\begin{aligned}(\overline{U}\overline{W})_\xi + (\overline{W}^2)_\eta + \overline{p}^*_\eta - \frac{J_\xi}{J}\overline{U}\overline{W} + \frac{J_\eta}{2J}(\overline{U}^2 - \overline{W}^2) \\ = K[(J^{\frac{1}{2}}\overline{W})_{\xi\xi} + (J^{\frac{1}{2}}\overline{W})_{\eta\eta}] + [(J^{\frac{1}{2}}\overline{W})_\eta - (J^{\frac{1}{2}}\overline{U})_\xi]\left[K_\eta - \frac{KJ_\eta}{J}\right] \\ + [(J^{\frac{1}{2}}\overline{U})_\eta + (J^{\frac{1}{2}}\overline{W})_\xi]\left[K_\xi - \frac{KJ_\xi}{J}\right]. \quad (2.13)\end{aligned}$$

Continuity: $$(J^{-\frac{1}{2}}\overline{U})_\xi + (J^{-\frac{1}{2}}\overline{W})_\eta = 0. \tag{2.14}$$

Turbulent energy:

$$\begin{aligned}(\overline{U}\bar{E})_\xi + (\overline{W}\bar{E})_\eta - \frac{\bar{E}}{2J}[\overline{U}J_\xi + \overline{W}J_\eta] \\ = J^{-\frac{1}{2}}K[(J^{\frac{1}{2}}\overline{U})_\eta + (J^{\frac{1}{2}}\overline{W})_\xi]^2 + J^{\frac{1}{2}}(K\bar{E}_\eta)_\eta + J^{\frac{1}{2}}(K\bar{E}_\xi)_\xi \\ + J^{-\frac{1}{2}}K[(J^{\frac{1}{2}}\overline{U})_\xi - (J^{\frac{1}{2}}\overline{W})_\eta]^2 - J^{-\frac{1}{2}}\frac{(\lambda\bar{E})^2}{K},\end{aligned} \tag{2.15}$$

where $\overline{p^*} = \overline{p} + \frac{2}{3}\bar{E}$.

In the turbulent energy equation, the dissipation ϵ has been assumed to be equal to $(\lambda\bar{E})^2/K \equiv (\lambda\bar{E})^{\frac{3}{2}}/l$, and the diffusive fluxes have been assumed to be of a gradient form given by

$$\overline{u'p'} + \overline{u'E'} = -J^{\frac{1}{2}}K\bar{E}_\xi, \quad \overline{w'p'} + \overline{w'E'} = -J^{\frac{1}{2}}K\bar{E}_\eta. \tag{2.16}$$

3. Boundary conditions and numerical method

In most turbulent boundary layers the appropriate vertical co-ordinate is

$$\mu = \ln\left(\frac{\eta + z_0}{z_0}\right), \tag{3.1}$$

and so (2.12)–(2.15) were transformed to a ξ, μ system prior to their numerical solution in the rectangle

$$0 \leqslant \xi \leqslant L, \quad 0 \leqslant \mu \leqslant \ln\left(\frac{H + z_0}{z_0}\right). \tag{3.2}$$

Here $\eta = H$ is the top of the integration region. We have taken $H \simeq 1{\cdot}2L$ in most of the runs as tests with deeper regions showed only small changes. The equations were solved in a frame of reference moving with the waves at speed c. If we make allowance for the first-order velocities in the wave itself, assuming irrotational flow, the boundary conditions on the Cartesian velocities (U_c, W_c) at the lower boundary can be written as

$$\left.\begin{aligned}U_c &= -c[1 + ak\cos k\xi] + O(ak)^2, \\ W_c &= -cak\sin k\xi + O(ak)^2.\end{aligned}\right\} \tag{3.3}$$

In terms of $\overline{U}, \overline{W}$ parallel to the ξ, μ co-ordinates this gives the boundary conditions to be imposed as

$$\left.\begin{aligned}J^{\frac{1}{2}}\overline{U} = -c, \quad \overline{W} = 0, \quad \bar{E}_\mu = 0 \quad \text{at} \quad \mu = 0, \\ \tau = u_0^2, \quad \overline{W} = 0, \quad \bar{E} = u_0^2/\lambda \quad \text{at} \quad \mu = \ln\left(\frac{H + z_0}{z_0}\right).\end{aligned}\right\} \tag{3.4}$$

The boundary condition of no flux of turbulent energy into the wave was thought to be the most appropriate to describe the physical situation. If $\tau = \lambda\bar{E}$ were used as an alternative, appropriate to the constant-flux layer very close to the surface, the boundary condition would be slightly different since $\tau_\mu \neq 0$ at the water surface. Computations made with the two boundary conditions showed changes in the results of less than 1 %. We also require periodicity in x or ξ so that

all variables have the same value at $\xi = 0$ and L. Velocities were scaled with respect to the friction velocity u_0 and lengths with respect to the surface roughness z_0 to give a non-dimensional set of equations. The method used to solve the equations is based on the technique of artificial compressibility due to Chorin (1967), which introduces time derivatives into (2.12), (2.13) and (2.15). An initial profile was set up with

$$\overline{U}_I = (\mu/\kappa) - c, \quad \overline{W} = 0, \quad \overline{p^*} = 0, \quad \overline{E}_I = 1/\lambda \tag{3.5}$$

everywhere and then the program marched forward in time determining new values of $\overline{U}$, $\overline{E}$ and $\overline{W}$ until a steady state was achieved. The updated pressure field is found from (2.14) in the form

$$\frac{1}{\alpha J}\overline{p_t^*} + (J^{-\frac{1}{2}}\overline{U})_\xi + (J^{-\frac{1}{2}}\overline{W})_\eta = 0, \tag{3.6}$$

where the artificial compressibility factor α must satisfy

$$\alpha^{\frac{1}{2}} > \max[\overline{U}, \overline{W}], \tag{3.7}$$

i.e. the flow must be subsonic with respect to the artificial sound speed $\alpha^{\frac{1}{2}}$. The integration technique uses a block iterative method in the vertical so that the stability restriction on the time step is only governed by the horizontal grid spacing. For a typical case we found that about 8000 cycles were needed to reach a steady state taking 2 min of CDC 7600 time with a 10×10 grid. Test runs were made using a finer, 20×14 grid but the results were essentially unchanged and the coarser grid has been used to reduce the computer time used. A steady state was judged to have been reached when the results changed by less than $\frac{1}{2}$ % over the last thousand cycles. Checks on the results were that the pressure field decayed away to zero at the top of the model and that an overall momentum balance was satisfied. In particular, the average horizontal force on the waves due to normal pressure and shear stress should sum to u_0^2. This was achieved to within about 2 % with the 10×10 grid.

4. Results

All results presented here are for

$$R \equiv -\ln(kz_0) = 8, \tag{4.1}$$

following Townsend's (1972) notation. If we take $z_0 = 0{\cdot}01$ cm, the waves then have $L = 1{\cdot}873$ m and $c = (g/k)^{\frac{1}{2}} = 1{\cdot}71$ m/s. This value of z_0 gives $U_5 \simeq 27u_0$, where U_5 is the velocity at a height of 5 m calculated from the logarithmic formula

$$\frac{U_5}{u_0} = \frac{1}{\kappa}\ln\left(\frac{z_5 + z_0}{z_0}\right), \tag{4.2}$$

for flow over a plane surface. The depth of the integration region is 2·2 m. If $c = 8u_0$ then $u_0 = 21{\cdot}4$ cm/s and $U_5 = 5{\cdot}78$ m/s while if $c = 12u_0$, $u_0 = 14{\cdot}25$ cm/s and $U_5 = 3{\cdot}86$ m/s.

We first look at the results of a typical case, chosen to be $c = 8u_0$ and

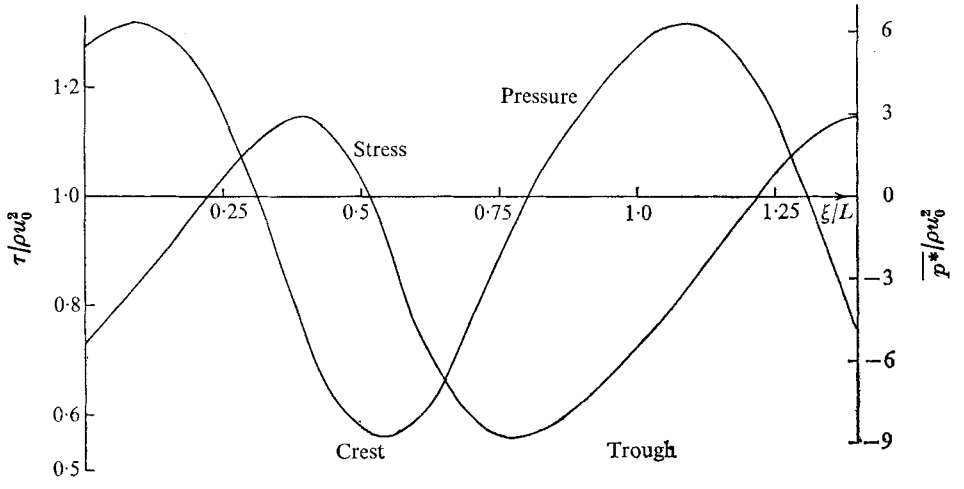

FIGURE 1. Surface pressure and shear stress. $R = 8$, $c = 8u_0$, $ak = 0{\cdot}157$, constant z_0.

$a = 0{\cdot}025L$ ($ak = 0{\cdot}157$). Figure 1 shows the surface pressure and shear stress distributions plotted against ξ/L. Both curves show considerable differences from the pure sinusoidal form of the lower boundary. This is especially noticeable in shear stress, where the distribution shows a distinct asymmetry with the extrema separated in the ratio 0·38:0·62 measured in terms of ξ/L. This asymmetry increases with wave amplitude. As ak increases the pressure minimum remains virtually fixed just forward of the crest, but the pressure maximum, which starts almost exactly 180° out of phase with the minimum when ak is small, migrates forwards from the wave trough, thereby causing the field to become asymmetric. Figure 2 shows contours of shear stress. The most interesting features are the elevated extrema, which occur roughly 180° out of phase with the surface extrema. The elevated minimum is over the wave crest and the elevated maximum over the wave trough. The elevated extrema occur at a height of about $0{\cdot}1L$ and are much more extensive than the surface features – note that figure 2 has a logarithmic vertical scale. Thus the elevated stress pattern is much more likely to be observed in any field measurements of stress since, in order to reveal surface features, measurements would have to be made within about $0{\cdot}005L$ of the wave surface. Turbulent energy contours are plotted in figure 3 and show the same general features as those of shear stress with all four extrema in very similar positions. The biggest difference is that the elevated extrema of turbulent energy are not as extreme as those of shear stress. This was also found in the case of flow over a fixed boundary (see Taylor *et al.* 1976).

Figure 4 is a plot of $(\overline{U} - \overline{U}_I)/u_0$ against μ where $\overline{U}_I$ is the initial profile defined in (3.5), which would be the profile if the surface was flat. Near the top of the model $\overline{U}$ has returned to a logarithmic form, so that $\overline{U} - \overline{U}_I$ is a constant. This difference, which is due to the form drag of the surface, is always negative when z_0 is constant and increases monotonically with increasing amplitude. It is found to be virtually independent of c/u_0. In figure 4 the difference is $-1{\cdot}35u_0$, so that the value of U_5 when $ak = 0{\cdot}157$ should be reduced by 5 % compared with the value

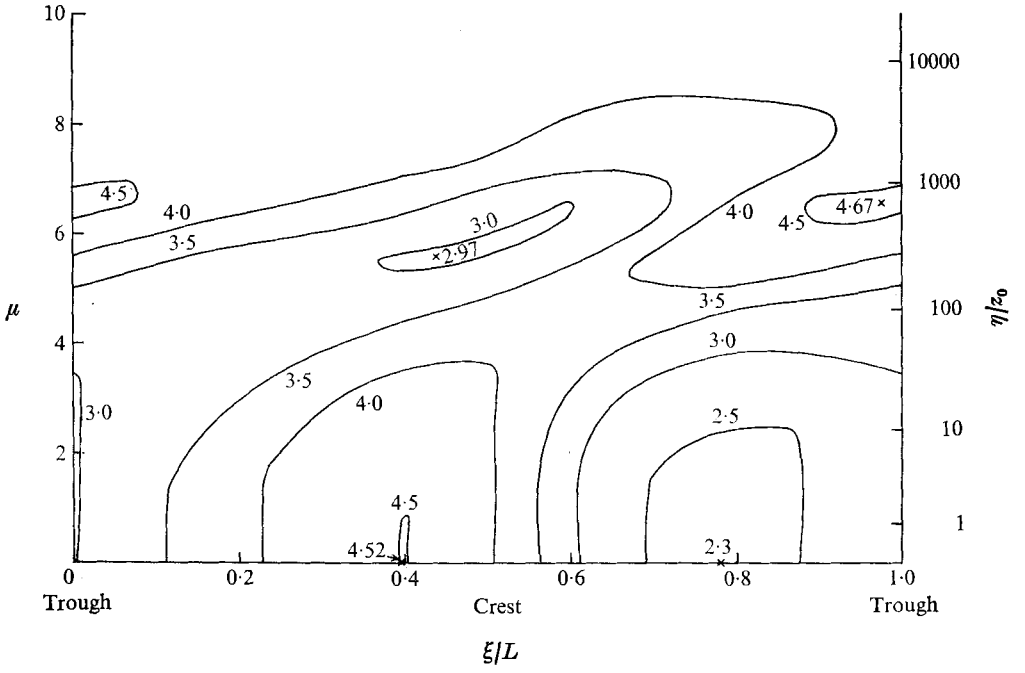

FIGURE 2. Shear stress contours, same run as figure 1.

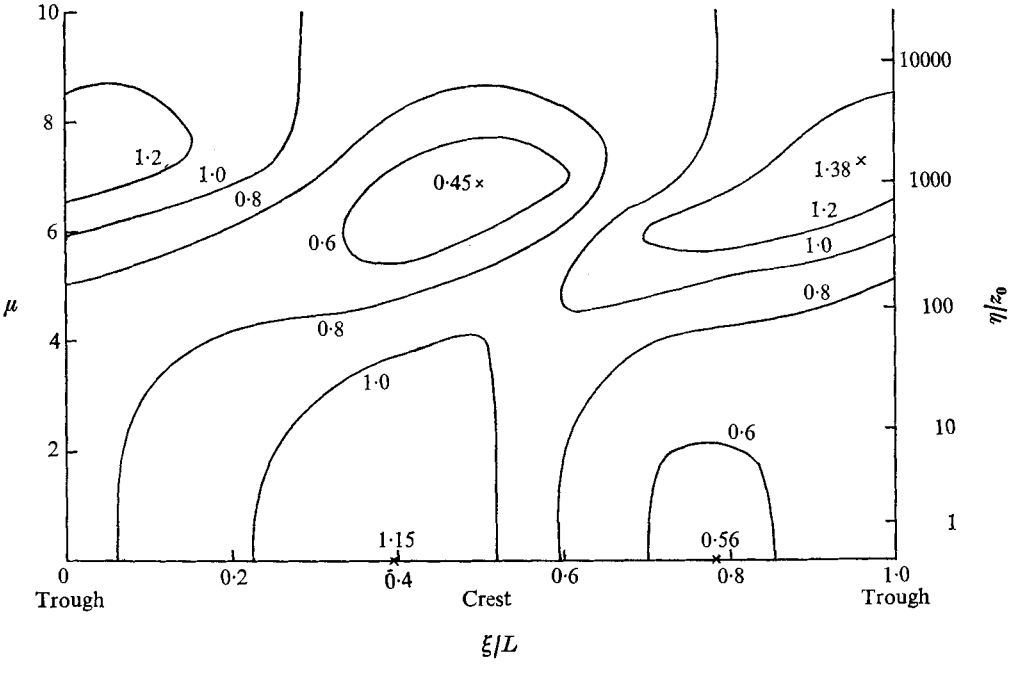

FIGURE 3. Contours of turbulent kinetic energy, same run as figure 1.

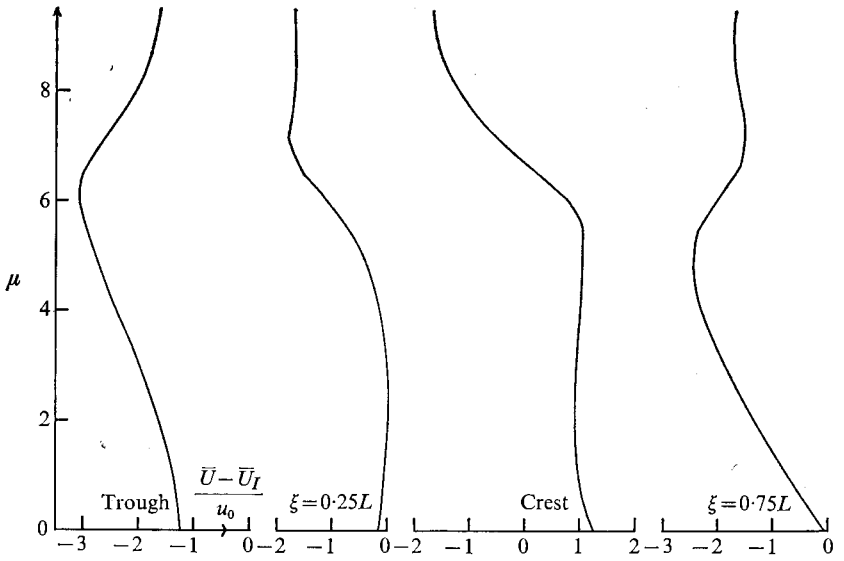

FIGURE 4. Horizontal velocity $(\bar{U}-\bar{U}_I)/u_0$ plotted against height, same run as figure 1.

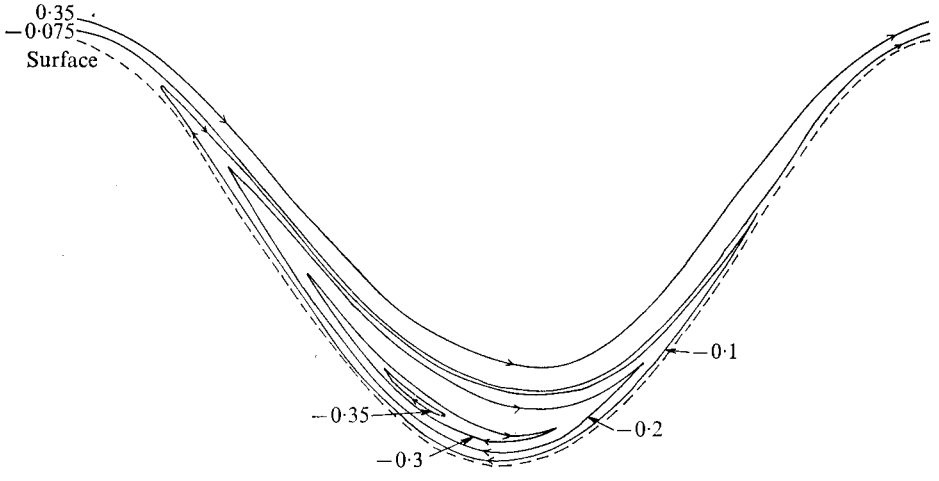

FIGURE 5. Streamlines in the wave trough, same run as figure 1. Vertical scale × 10.

of $27u_0$ over a flat surface. Figure 4 also shows that matching the first-order water particle velocities in the wave means that $\bar{U}-\bar{U}_I$ at the surface is negative in the trough but positive at the crest. Near the surface the velocity shear is larger at the crest than at the trough but above $\mu = 5{\cdot}5$ or a height of $0{\cdot}015L$ the situation reverses with the larger shear over the trough. Figure 5 shows some streamlines of the flow calculated from

$$\int_{z_b}^{z} (U_c - c)\, dz$$

and plotted in x and z. The vertical scale is multiplied by a factor of ten, and the frame of reference is travelling with the waves. The figure shows a region of closed streamlines in the wave trough. This is deepest about 36° backwards from the trough itself and at this point is $0{\cdot}01L$ or $0{\cdot}4a$ deep. The depth and height above the wave of the region of closed streamlines depends critically upon the phase speed of the wave c. When c/u_0 is small the region is thin and occurs just above the wave surface. As c/u_0 increases, however, the region becomes deeper and also occurs much higher above the surface, so that when $c = 20u_0$ the region of closed streamlines starts around $0{\cdot}1L$ and has a maximum depth of $0{\cdot}15L$. It may be remarked, however, that for reasonable values of c/u_0, velocity measurements must be made very close to the surface, certainly within a small fraction of the wave amplitude, in order to be able to detect the region of closed streamlines predicted by this model.

Two series of runs have been made with fixed values of c/u_0 and increasing amplitude. The results are given in tables 1 and 2. From table 1, with $c = 8u_0$, we note that for small amplitude the phase of the pressure maximum forward from its equilibrium position over the trough is 16° whereas Townsend predicts 11°. The position of the pressure maximum is important in determining the rate of energy input to the wave by the normal pressure $(\langle -c(\overline{p}+\overline{w'^2})\,(dz_b/dx)\rangle$, where the angle brackets denote an average over the wave form). The nearer the pressure maximum is to 90° forward of the trough the greater the amount of work that can be done on the wave. Table 1 clearly shows that the phase shift forwards from the trough increases with wave amplitude and reaches a value of 83° when $ak = 0{\cdot}314$. Attempts to obtain results for $ak > 0{\cdot}314$ have been unsuccessful, and even at $0{\cdot}314$, the results are becoming unsatisfactory. The magnitude of the pressure wave increases up to a maximum when ak is about $0{\cdot}157$ and then decreases again. Expressed as a multiple of ak, however, it decreases monotonically as ak increases. This combination, of a favourable phase shift but decreasing amplitude for the pressure, results in a decrease in the fractional rate of energy gain per radian advance in phase, ζ, as ak increases. Table 2, with $c = 12u_0$, reveals a similar pattern with the fractional rate of energy supply falling slowly with increasing amplitude as the pressure phase increases towards 90° but then decreasing rapidly as the pressure maximum moves forwards past the optimum position. It should be noted, however, that the quantities are scaled with respect to the total horizontal stress on the water surface, u_0^2, and that this could be expected to increase slightly with increasing wave amplitude if, for example, U_5 were regarded as fixed. The values of the pressure contribution p_x in tables 1 and 2 can be interpreted as the rate of energy supply as a proportion of the maximum possible, $\rho_{\mathrm{air}} u_0^2 c$. We note that although ζ decreases as ak increases, this is inevitable if u_0 is regarded as fixed, since the wave energy is proportional to a^2. For $ak = 0{\cdot}157$, figures of 20 % and above for the proportion of the available energy going into the waves are very satisfactory.

The phase of the surface shear stress maximum is measured from the wave crest and the results confirm Townsend's (1972) conclusion that both pressure and stress maxima occur on the backward slope of the wave. Increasing amplitude has less effect on the surface stress than on the pressure in the sense that the

ak Townsend	Phase of pressure maximum from trough in x		$\frac{p_{max}-p_{min}}{\rho u_0^2}$	Phase of stress maximum from crest in x		$\frac{\tau_{max}-\tau_{min}}{\rho u_0^2}$	Pressure contribution p_x	Fractional rate of energy supply Units $\frac{\rho_{air}}{\rho_{water}}\left(\frac{u_0}{c}\right)^2\zeta = \frac{2p_x}{(ak)^2}$
$<0{\cdot}1$	0·031	11·2°	$122ak$	−0·125	−45°	$4{\cdot}8ak$	$5{\cdot}92\,(ak)^2$	11·84
0·01	0·045	16·2°	$1{\cdot}35\,(135ak)$	−0·144	−51·9°	$0{\cdot}043\,(4{\cdot}3ak)$	0·0009	18
0·05	0·054	19·4°	$6{\cdot}45\,(129ak)$	−0·127	−45·9°	$0{\cdot}218\,(4{\cdot}3ak)$	0·022	17·4
0·1	0·07	25°	$11{\cdot}6\,(116ak)$	−0·112	−40·3°	$0{\cdot}42\,(4{\cdot}2ak)$	0·083	16·6
0·157	0·098	35°	$14{\cdot}7\,(93{\cdot}6ak)$	−0·099	−35·8°	$0{\cdot}59\,(3{\cdot}8ak)$	0·19	15·4
0·226	0·146	52°	$11{\cdot}8\,(52{\cdot}6ak)$	−0·092	−33·3°	$0{\cdot}67\,(3ak)$	0·34	13·5
0·314	0·231	83·2°	$8{\cdot}1\,(25{\cdot}8ak)$	−0·097	−35°	$0{\cdot}59\,(1{\cdot}9ak)$	0·56	11·35

TABLE 1. $R = 8$, $c = 8u_0$, z_0 constant

ak Townsend	Phase of pressure maximum from trough in x		$\frac{p_{max}-p_{min}}{\rho u_0^2}$	Phase of stress maximum from crest in x		$\frac{\tau_{max}-\tau_{min}}{\rho u_0^2}$	Pressure contribution p_x	Fractional rate of energy supply Units $\frac{\rho_{air}}{\rho_{water}}\left(\frac{u_0}{c}\right)^2\zeta = \frac{2p_x}{(ak)^2}$
$<0{\cdot}1$	0·174	62·6°	$41{\cdot}5\,ak$	−0·253	−91·1°	$4{\cdot}46ak$	$9{\cdot}2\,(ak)^2$	18·4
0·01	0·148	53·4°	$0{\cdot}43\,(43ak)$	−0·269	−96·8°	$0{\cdot}04\,(4ak)$	0·0009	18
0·05	0·162	58·4°	$2{\cdot}07\,(41{\cdot}4ak)$	−0·259	−93·1°	$0{\cdot}2\,(4ak)$	0·021	16·9
0·1	0·188	67·7°	$3{\cdot}67\,(36{\cdot}7ak)$	−0·258	−92·9°	$0{\cdot}38\,(3{\cdot}8ak)$	0·082	16·5
0·157	0·232	85°	$5{\cdot}1\,(32{\cdot}5ak)$	−0·282	−101·7°	$0{\cdot}56\,(3{\cdot}6ak)$	0·19	15·4
0·226	0·317	114·1°	$5{\cdot}9\,(26{\cdot}3ak)$	−0·326	−117·4°	$0{\cdot}73\,(3{\cdot}3ak)$	0·32	12·7
0·314	0·362	130·2°	$5{\cdot}2\,(16{\cdot}6ak)$	−0·357	−128·6°	$0{\cdot}94\,(3ak)$	0·39	7·95

TABLE 2. $R = 8$, $c = 12u_0$, z_0 constant

ak	c/u_0	Phase of pressure maximum from trough in x		$\frac{p_{max}-p_{min}}{\rho u_0^2}$	Phase of stress maximum from crest in x		$\frac{\tau_{max}-\tau_{min}}{\rho u_0^2}$	Pressure contribution p_x	Fractional rate of energy supply Units $\frac{\rho_{air}}{\rho_{water}}\left(\frac{u_0}{c}\right)^2\zeta = \frac{2p_x}{(ak)^2}$
0·01	4	0·025	8·9°	2·92 (292ak)	−0·094	−33·7°	0·068 (6·8ak)	0·001	20
0·157	4	0·048	17·3°	35·6 (226ak)	−0·063	−22·6°	0·86 (5·5ak)	0·217	17·6
0·01	6	0·031	11·3°	2·05 (205ak)	−0·11	−40°	0·055 (5·5ak)	0·001	20
0·157	6	0·065	23·5°	24·2 (154ak)	−0·076	−27·5°	0·71 (4·5ak)	0·2	16·3
0·01	10	0·075	27°	0·76 (76ak)	−0·2	−71·5°	0·039 (3·9ak)	0·0008	16
0·157	10	0·152	54·8°	7·71 (49ak)	−0·16	−58·5°	0·51 (3·2ak)	0·186	15·1
0·01	14	0·234	84·3°	0·35 (35ak)	−0·33	−121·1°	0·047 (4·7ak)	0·0009	18
0·157	14	0·31	111·4°	4·13 (26·3ak)	−0·36	−128·7°	0·7 (4·5ak)	0·164	13.3
0·01	16	0·26	93·6°	0·276 (27·6ak)	−0·392	−141·2°	0·059 (5·9ak)	0·0007	14
0·157	16	0·276	100°	2·8 (17·8ak)	−0·393	−141·5°	0·85 (5·4ak)	0·11	8·6
0·01	18	0·182	65·4°	0·17 (17ak)	−0·418	−150·4°	0·067 (6·7ak)	0·0004	8
0·157	18	0·12	43·1°	2·59 (16·5ak)	−0·411	−148·1°	1·0 (6·34ak)	0·0434	3.52
0·01	20	0·003	1·2°	0·22 (22ak)	−0·431	−155·1°	0·076 (7·6ak)	0	0
0·157	20	−0·033	−12°	4·48 (28·5ak)	−0·418	−150·5°	1·156 (7·36ak)	−0·144	−1·16

TABLE 3. $R = 8$, z_0 constant

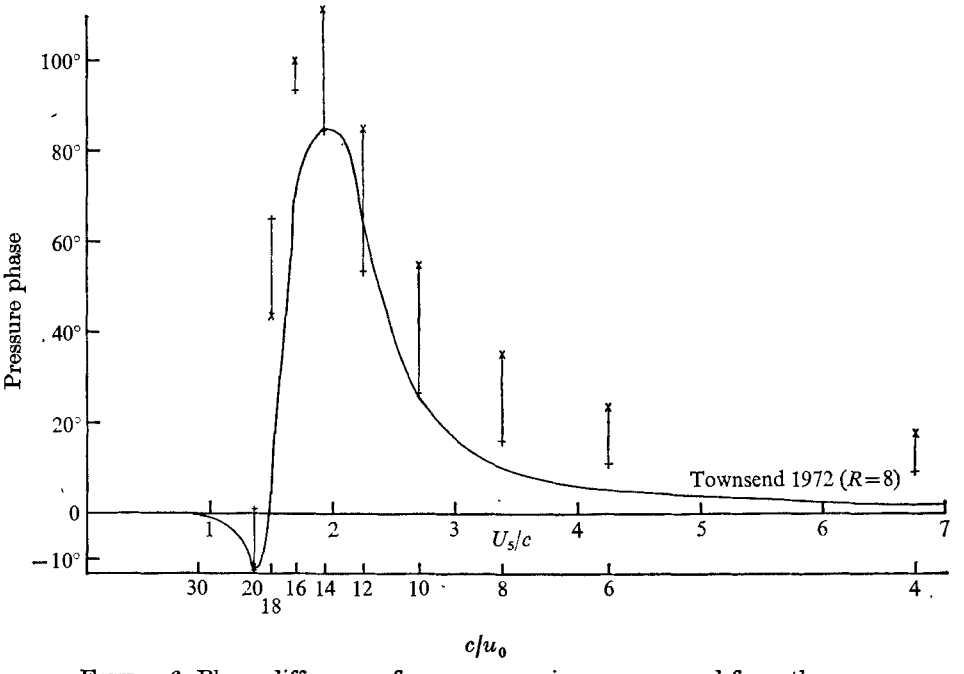

FIGURE 6. Phase difference of pressure maximum measured from the wave trough against U_5/c. Constant z_0; +, $ak = 0{\cdot}01$; ×, $ak = 0{\cdot}157$.

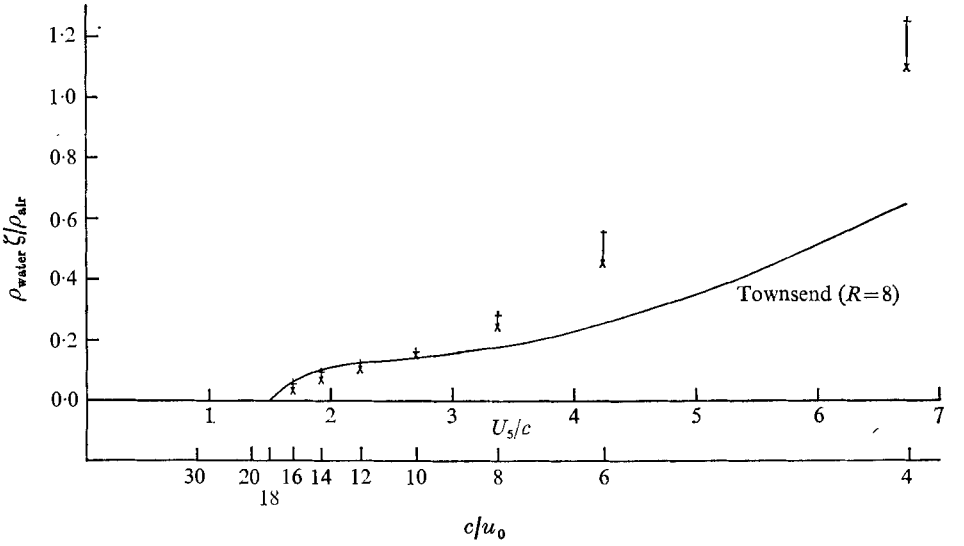

FIGURE 7. Fractional rate of energy gain per radian advance in phase, ζ, against U_5/c. Same notation as figure 6.

position of the stress maximum and the magnitude of the stress field, expressed as a multiple of ak, change little. Thus our results for shear stress, in this respect, agree with those from a linear theory which predicts a fixed phase shift and fixed magnitude, expressed as a multiple of ak, for all wave amplitudes. A simple linear theory, however, is unable to predict the considerable distortion from a sinusoidal form found in our surface stress distributions.

Table 3 shows other runs at various values of c/u_0. If we regard z_0 and the wavelength as fixed, this determines c through the dispersion relation, and changes in c/u_0 represent changes in the value of u_0 and hence in the wind speed U_5 at 5 m. For these results, the phase shift of the pressure maximum is plotted against U_5/c in figure 6 and is compared with Townsend's (1972) results. The lines shown joining the phases for $ak = 0{\cdot}01$ and $0{\cdot}157$ are intended to indicate the range for intermediate values of ak. However, intermediate values may lie outside the limits shown, and this occurs, for example, when $c = 16u_0$ on figure 6. The results show a very rapid movement of the pressure maximum from near zero when $c = 20u_0$ to a maximum of about 90° when $c = 16u_0$. The phase shift then gradually reduces as c/u_0 decreases further. In order to present our results in terms of both U_5/c and c/u_0 we have set $U_5 = 27u_0$, the value for flow over a plane surface with $z_0 = 0{\cdot}01$ cm, rather than adjusting it for each amplitude. Figure 7 shows the predicted rate of energy gain per radian advance in phase, ζ, plotted against U_5/c. We again anticipate that values of ak between $0{\cdot}01$ and $0{\cdot}157$ will usually give intermediate values of ζ. Note that the higher values of ζ correspond to the lower values of ak. These ζ values are significantly higher than those found by Townsend for $U_5/c > 4$ owing to differences in the predicted pressure phase for these cases.

5. Variable roughness length

In order to try to model the effect of small capillary and short gravity waves which are often present near the crest of larger waves, z_0 was allowed to vary with ξ, taking the form

$$z_0 = \bar{z}_0[1 - \gamma \cos(k\xi - \delta)]; \tag{5.1}$$

$\bar{z}_0$ is now the average value of z_0 and is used as the length to non-dimensionalize the equations. Variable z_0 was introduced into the program by using a wall-layer approximation for the bottom three grid points of the finite-difference mesh. Three grid points were used as the best balance between using a shallow enough region where the wall-layer approximation is valid, and a deep enough region to incorporate the effects of varying z_0. The depth is approximately $20z_0$. In the wall layer equation (2.12) is approximated by

$$\frac{\overline{p_\xi^*}}{J} = \left(\frac{K}{J}(J^{\frac{1}{2}}\overline{U})_\eta\right)_\eta \tag{5.2}$$

using a boundary-layer approximation where vertical derivatives are much larger than horizontal derivatives and $\overline{U} \gg \overline{W}$. If $\overline{p_\xi^*}/J$ is assumed independent of η in the wall layer and if ϕ is defined such that $\phi(\xi) \equiv \overline{p_\xi^*}$, then (5.2) can be integrated with respect to η to give

$$K(J^{\frac{1}{2}}\overline{U})_\eta = \phi\eta + \tau_0, \tag{5.3}$$

ak	c/u_0	γ	Phase of pressure maximum from trough in x		$\frac{p_{max}-p_{min}}{\rho u_0^2}$	Phase of stress maximum from crest in x		$\frac{\tau_{max}-\tau_{min}}{\rho u_0^2}$	Pressure contribution p_x	Fractional rate of energy supply Units $\frac{\rho_{air}}{\rho_{water}}\left(\frac{u_0}{c}\right)^2\zeta = \frac{2p_x}{(ak)^2}$
0·01	6	0·5	0·093	33·4°	2·47 (247ak)	0·08	28·7°	0·335 (33·5ak)	0·0032	64
0·157	6	0·75	0·077	27·7°	24·4 (155ak)	−0·033	−11·8°	0·782 (5ak)	0·241	19·5
0·01	8	0·5	0·116	41·7°	1·95 (195ak)	0·097	34·8°	0·308 (30·8ak)	0·0031	62
0·05	8	0·6	0·078	28·2°	7·16 (143ak)	0·007	2·4°	0·407 (8·1ak)	0·035	28·1
0·157	8	0·75	0·109	39·2°	15·35 (97·7ak)	−0·044	−15·8°	0·57 (3·6ak)	0·231	18·7
0·01	10	0·5	0·132	47·4°	1·66 (166ak)	0·12	44·7°	0·284 (28·4ak)	0·003	60
0·157	10	0·75	0·148	53·4°	9·0 (57·3ak)	−0·068	−24·5°	0·358 (2·28ak)	0·225	18·2
0·01	12	0·5	0·13	47°	1·41 (141ak)	0·161	57·9°	0·276 (27·6ak)	0·0026	52
0·05	12	0·6	0·144	51·9°	3·29(65·7ak)	0·042	15°	0·225(4·5ak)	0·0314	25·1
0·157	12	0·75	0·197	70·7°	6·0 (38·2ak)	−0·108	−38·8°	0·228 (1·45ak)	0·218	17·6
0·01	14	0·5	0·098	35·2°	1·08 (108ak)	0·194	69·9°	0·308 (30·8ak)	0·0017	34
0·157	14	0·75	0·253	90·9°	4·7 (30ak)	0·409	147·1°	0·4 (2·55ak)	0·18	14·6
0·01	16	0·5	0·03	10·9°	0·66 (66ak)	0·204	73·3°	0·35 (35ak)	0·0003	6
0·157	16	0·75	0·259	93·2°	3·12 (19·9ak)	0·4	144·3°	0·55 (3·5ak)	0·115	9·3
0·01	18	0·5	−0·056	−20·3°	0·32 (32ak)	0·201	72·4°	0·37 (37ak)	−0·0003	−6
0·157	18	0·75	0·167	60·1°	2·4 (15·3ak)	0·4	144°	0·72 (4·6ak)	0·056	4·56
0·01	20	0·5	−0·052	−18·9°	0·19 (19ak)	0·202	72·7°	0·37 (37ak)	−0·0001	−2
0·157	20	0·75	−0·019	−6·9°	3·52 (22·4ak)	0·402	144·7°	0·88 (5·6ak)	−0·0025	−0·2

TABLE 4. $R = 8$, $\delta = \frac{1}{4}\pi$, variable z_0

c/u_0	δ	Phase of pressure maximum from trough in x		$\frac{p_{max}-p_{min}}{\rho u_0^2}$	Phase of stress maximum from crest in x		$\frac{\tau_{max}-\tau_{min}}{\rho u_0^2}$	Pressure contribution p_x	Fractional rate of energy supply Units $\frac{\rho_{air}}{\rho_{water}}\left(\frac{u_0}{c}\right)^2\zeta = \frac{2p_x}{(ak)^2}$
8	0	0·057	20·3°	2·91 (291ak)	−0·014	−4·9°	0·54 (54ak)	0·0027	54
8	$\frac{1}{4}\pi$	0·14	49·6°	2·54 (254ak)	0·103	37·2°	0·502 (50·2ak)	0·0045	90
8	$\frac{1}{2}\pi$	0·222	79·8°	1·8 (180ak)	0·239	85·9°	0·45 (45ak)	0·0042	84
12	0	0·021	7·7°	1·93 (193ak)	0·03	10·8°	0·5 (50ak)	0·0009	18
12	$\frac{1}{4}\pi$	0·13	47°	2·05 (205ak)	0·166	59·8°	0·467 (46·7ak)	0·0037	74
12	$\frac{1}{2}\pi$	0·237	85·2°	1·96 (196ak)	0·309	111·4°	0·48 (48ak)	0·0048	96

TABLE 5. $R = 8$, $ak = 0{\cdot}01$, $\gamma = 0{\cdot}75$, variable z_0

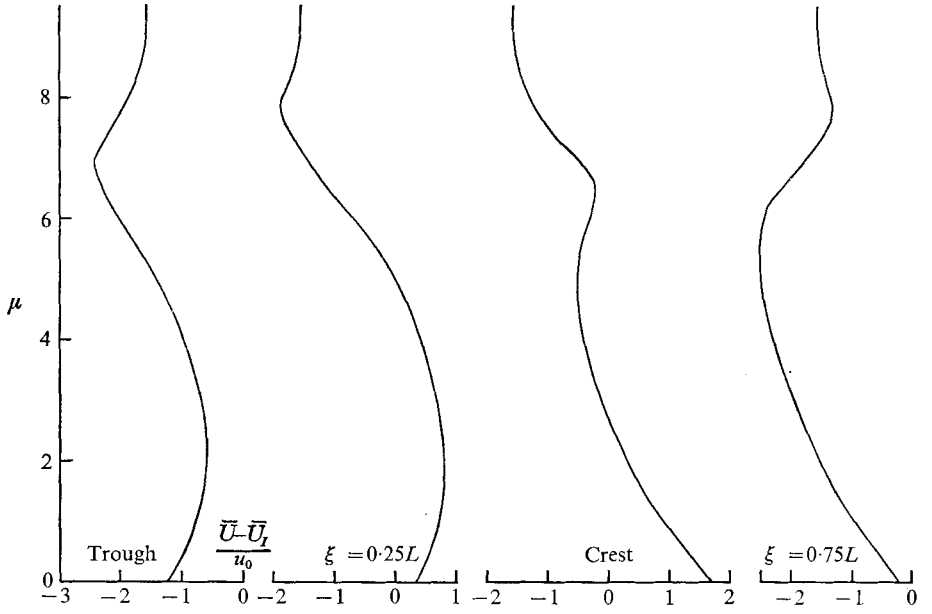

FIGURE 8. Horizontal velocity $(\bar{U}-\bar{U}_I)/u_0$ plotted against height for $R = 8$, $c = 12u_0$, $ak = 0{\cdot}157$, $\gamma = 0{\cdot}75$ and $\delta = \frac{1}{4}\pi$.

where $\tau_0(\xi)$ is the surface shear stress. The dominant terms retained in the turbulent energy equation (2.15) are the production and dissipation terms, so that

$$J^{-\frac{1}{2}}K[(J^{\frac{1}{2}}\bar{U})_\eta]^2 = J^{-\frac{1}{2}}(\lambda\bar{E})^2/K. \tag{5.4}$$

Taking the square root gives

$$\lambda\bar{E} = K(J^{\frac{1}{2}}\bar{U})_\eta = \phi\eta + \tau_0, \tag{5.5}$$

or $\tau = \lambda\bar{E}$ in the wall layer. Elimination of $\bar{E}$ gives an equation for $J^{\frac{1}{2}}\bar{U}$ which, when $\tau_0 \gg \phi\eta$, can be integrated to give

$$J^{\frac{1}{2}}\bar{U} = \frac{(J\tau_0)^{\frac{1}{2}}}{\kappa}\ln\left(\frac{J^{-\frac{1}{2}}\eta + z_0}{z_0}\right) + \frac{\phi}{2\kappa}\left(\frac{J}{\tau_0}\right)^{\frac{1}{2}}\left[\eta - z_0 J^{\frac{1}{2}}\ln\left(\frac{J^{-\frac{1}{2}}\eta + z_0}{z_0}\right)\right] - c, \tag{5.6}$$

where z_0 is now taken as a function of ξ, and the length l is approximated by

$$l \approx \kappa(s + z_0) \approx \kappa(J^{-\frac{1}{2}}\eta + z_0). \tag{5.7}$$

The profiles of $\bar{U}$ and $\bar{E}$ within the wall layer were assumed to be of the form given by (5.5) and (5.6), but (5.5) now requires the lower boundary condition on turbulent energy to be

$$\bar{E} = \tau_0/\lambda \quad \text{at} \quad \mu = 0. \tag{5.8}$$

This boundary condition was used for mathematical convenience as no way could be found to introduce the wall-layer approximation with the boundary condition $\bar{E}_\mu = 0$.

In the absence of any precise observations, the phase δ of the surface roughness perturbation was given the value $\frac{1}{4}\pi$ so the maximum occurs 45° forward of the

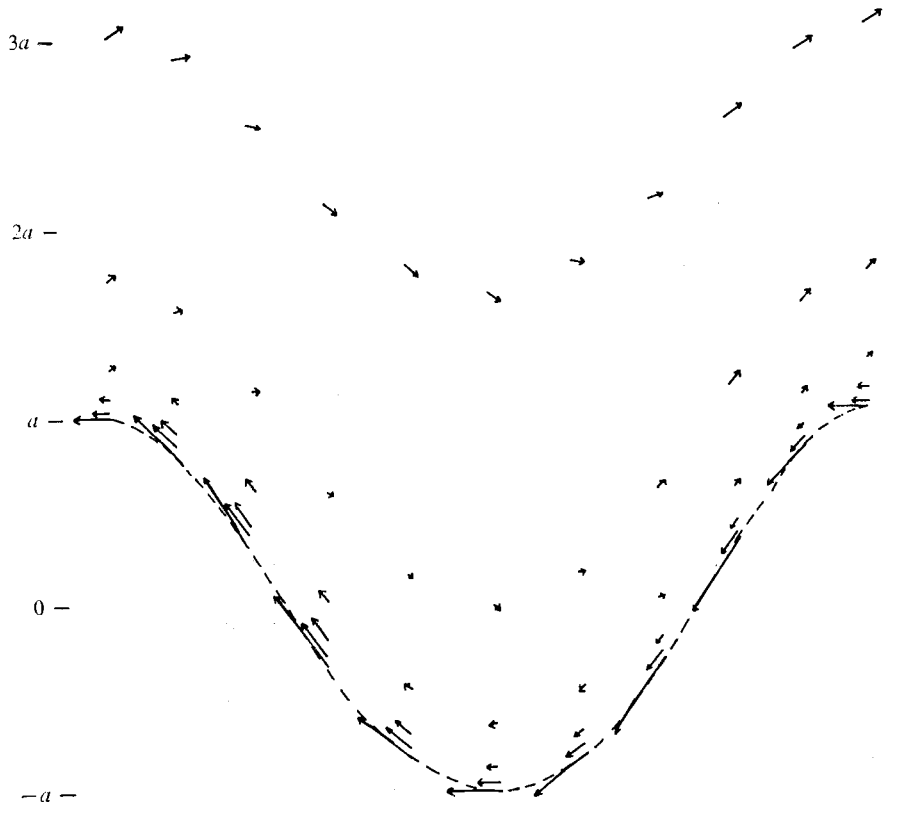

FIGURE 9. Cartesian velocities for same run as figure 8. Vertical scale × 10.

wave crest (see Keller & Wright 1975). The results of several runs are given in table 4. A few other runs were performed with $\delta = 0$ and $\frac{1}{2}\pi$ and these are listed in table 5. The amplitude γ of the z_0 variation could possibly be a large fraction of the mean value and initially we put $\gamma = 0{\cdot}75$. However, we felt this value to be rather high for very small amplitude waves and made further runs with $\gamma = 0{\cdot}5$ when $ak = 0{\cdot}01$ and $\gamma = 0{\cdot}6$ when $ak = 0{\cdot}05$ (see table 4). The results show that, for very small amplitude, the variable surface roughness has a dramatic effect upon the flow and upon the fractional rate of energy input. This can easily be made three times the value for constant z_0, and is five times greater in the extreme runs with $\gamma = 0{\cdot}75$ and $\delta = \frac{1}{2}\pi$. This stems from the distribution of pressure, which, for $8u_0 \leqslant c \leqslant 12u_0$ and small amplitude, is found to be nearly 180° out of phase with the z_0 distribution. This does not hold for larger values of c/u_0 (e.g. $c = 16u_0$) which lie outside the main generation region, when ζ is reduced. The effect of a variable z_0 reduces as the amplitude of the waves increases. When $ak = 0{\cdot}157$ the results shown in table 4, including the pressure phase shifts and the fractional rate of energy input, have returned close to the values predicted when z_0 is constant. Thus the relatively high rates of energy input found in these variable z_0 runs are confined to very small amplitude waves with $ak < 0{\cdot}03$ and

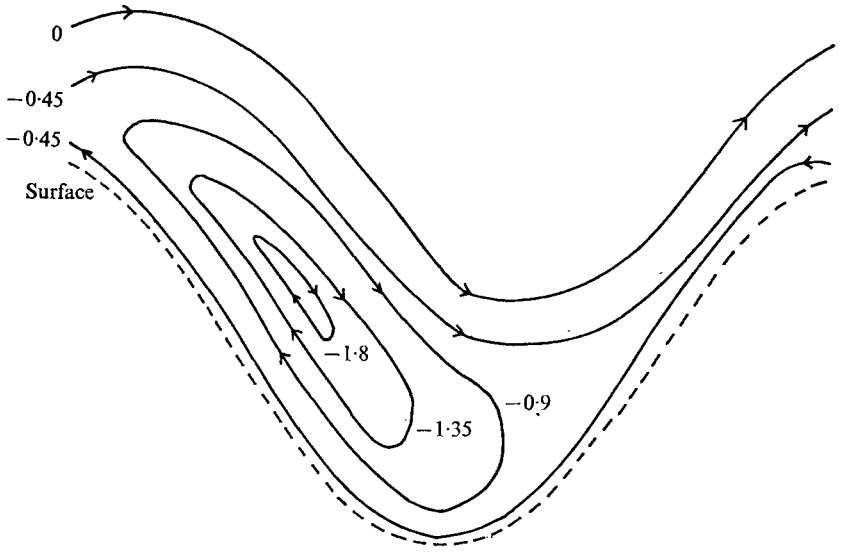

FIGURE 10. Streamlines for the same run as figure 8. Vertical scale × 10.

$8u_0 \leqslant c \leqslant 12u_0$. The main change to the flow field is in the horizontal velocity profiles near the water surface.

Figure 8 shows $(\overline{U}-\overline{U}_I)/u_0$ against height for $c = 12u_0$, $ak = 0{\cdot}157$, $\gamma = 0{\cdot}75$ and $\delta = \frac{1}{4}\pi$. Although figure 4 has $c = 8u_0$, comparison with figure 8 shows that much larger and smaller shears occur in the variable z_0 computations at positions where the surface roughness has its minimum and maximum respectively.

Longuet-Higgins (1969*b*) points out the effects of a variable shear stress on the boundary layer just above the wave surface and upon the wave growth rate. We have calculated the rate of work being done by the shear stress in our runs and have found that it is significant only at very small amplitude. This is, however, assuming an irrotational flow field in the water with surface velocities given by (3.3) and could perhaps be larger if the surface water velocities were modified. For the variable z_0 runs with $ak = 0{\cdot}01$, the work done on the wave by shear stress was about 15 % of that done by pressure for $6u_0 \leqslant c \leqslant 14u_0$. When $ak = 0{\cdot}05$ the percentage has reduced to about 5% and when $ak = 0{\cdot}157$ it was found that in most cases a very small amount of energy was being transferred back from the wave to the air by the action of the shear stress.

Figure 9 shows Cartesian velocities in the frame of reference moving with the wave for the same run as figure 8. The vertical scale is increased tenfold and the arrows indicate the direction and magnitude of the velocity. It is interesting to note that the critical height (above the water surface), where the horizontal component of velocity is zero, is considerably smaller over the crest than over the trough. Figure 10 shows the streamline pattern from the same run and, compared with figure 5, shows a much thicker region of closed streamlines. This is a consequence of the higher value of c/u_0. The centre of the closed-streamline cell is slightly farther from the trough compared with the case with $c = 8u_0$ and z_0 constant.

For variable z_0, the pressure phases and fractional energy input rates appear to be closer to observations, although this statement cannot be made definitively because of the large scatter in observational results. A comparison is made in the next section.

6. Comparison with other studies

The present work can be considered as an extension of Townsend's (1972) linear theory. The differences between the predictions of the two studies for small amplitude waves are generally small and probably can be attributed to the different closure hypotheses used. However, there is a possibility that Townsend's linearized treatment of the lower boundary condition on horizontal velocity (equation (3.6) of his paper) may lead to some inaccuracy in his results. This would be most pronounced for the higher values of U_5/c. We find that linearization is only valid for ak less than about 0·05. For higher amplitudes, nonlinear effects give rise to changes in the magnitude and phase of the field quantities, especially pressure, as shown in tables 1, 2 and 3.

On the experimental side, the present theory of flow over a two-dimensional monochromatic wave is, perhaps, most appropriately compared to a laboratory situation where such a wave can be generated. In the sea, where a broader, two-dimensional spectrum of waves will be present, we need to be rather cautious in making direct comparisons in view of our claim that nonlinear effects can be important. Shemdin (1969), working a wind–water tunnel, has measured velocity profiles and pressure fields using wave-following instruments above essentially monochromatic waves with $ak \simeq 0{\cdot}1$. The streamline diagrams shown in Shemdin's report (figures 18–23) agree qualitatively with our findings. Both show a deep region of closed streamlines well above the wave surface when c/u_0 is large changing to a narrow closed-streamline region just above the wave surface when c/u_0 becomes small. In fact, Shemdin's figure 42 shows quite good agreement with our figure 5 in that the centre of the closed-streamline region is just backward from the wave trough. Despite this qualitative agreement all Shemdin's velocity profiles have a pronounced maximum at a height of about $0{\cdot}5a$ above the wave surface which is not present in any of our computations. One possible explanation for this velocity maximum and other differences with our theory is that the measurements were taken after the wind had blown over only one or two waves and so may not have had sufficient time to reach a steady state in the frame of reference moving with the wave. In later work Shemdin & Lai (1973) find a less pronounced velocity maximum. There is also evidence in their figures 48 and 50 to support our use of a variable roughness length since they show an increase and decrease in velocity shear at the wave trough and crest respectively as shown in our figure 8. Comparison with the pressure results is more difficult since Shemdin (1969) finds a large scatter in the Miles (1959) β parameter, which governs the fractional rate of energy input. Shemdin concludes, however, that when $c > 6u_0$ Miles' theory underestimates the fractional rate of energy input found in his experiments. This conclusion agrees with our results for a variable roughness length.

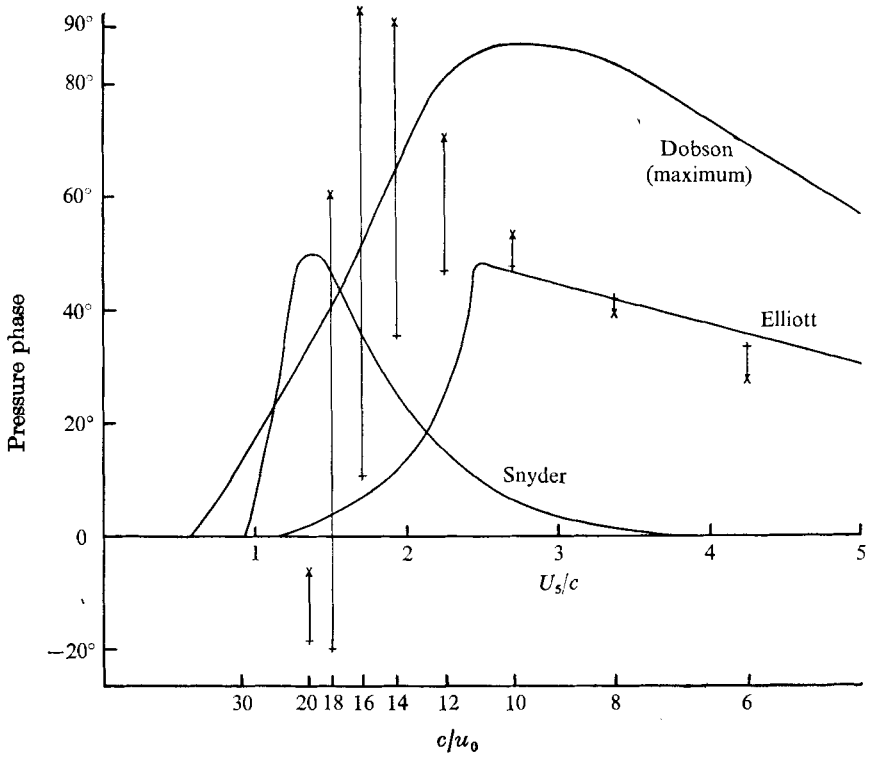

FIGURE 11. Phase difference of pressure maximum measured from wave trough against U_5/c. Variable z_0, $\delta = \frac{1}{4}\pi$. +, $ak = 0{\cdot}01, \gamma = 0{\cdot}5$; ×, $ak = 0{\cdot}157, \gamma = 0{\cdot}75$.

Another laboratory investigation was carried out by Kendall (1970), who measured the flow over twelve sinusoidal waves with $ak = 0{\cdot}196$. These were not water waves but were made from a smooth Neoprene sheet which could be made to move in a wavelike fashion. He obtained surface pressure measurements and plotted the phase shift of the pressure distribution compared with the wave trough against c/u_∞ in his figure 5 (*b*). When c is zero, he gives a value of 10°, which is close to our prediction of 13° when $c = 0$ and $ak = 0{\cdot}157$. Kendall's values for the phase shift increase to a value of 85° when $c = 0{\cdot}37u_\infty$ whereas table 2 shows that our predicted phase shift is 85° for $ak = 0{\cdot}157$ when $c = 12u_0$ or $c/U_5 = 0{\cdot}44$. Kendall's velocity and some shear stress results were obtained from instruments fixed at certain heights above the average wave surface. Thus observations could be taken very close to the wave crest but must always be at least $2a$ away from the trough. Measurements of horizontal velocity, his figure 7 (*b*), show large fluctuations near the wave crest mainly as a result of vertical shear. Similarly his figure 11 (*a*) shows shear stress measured along a horizontal line approximately $\frac{1}{2}a$ above the wave crest, and has a double peak. Similar features are found if we plot our results in this way but merely serve to illustrate how difficult it is to interpret measurements made at a fixed height compared with those from wave-following instruments. Altogether there seems to be reasonable agreement between our results and Kendall's (1970) observations.

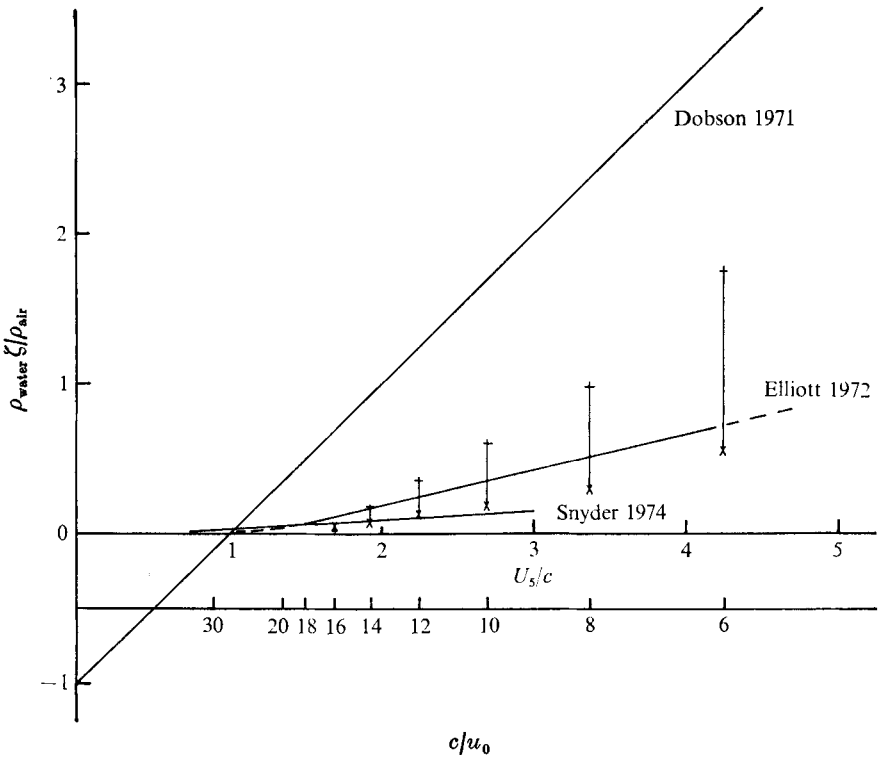

FIGURE 12. Fractional rate of energy gain per radian advance in phase, ζ, against U_5/c. Same notation as figure 11.

The observations of the wind wave generation process at sea include those of Dobson (1971), Elliott (1972) and Snyder (1974), who have measured, either directly or by extrapolation to the water surface, the rate of energy input to the waves. Using Fourier analysis, most have measured the phase lag of pressure components compared with the wave surface which, we predict, are dependent upon the wave amplitude. These phase lag results, including the maximum phase difference of Dobson, are summarized in figure 11, which shows the phase difference compared with the wave trough against U_5/c. Our results, for variable z_0 and $\delta = \frac{1}{4}\pi$, lie along the lines shown joining the results for $ak = 0{\cdot}01$ and $\gamma = 0{\cdot}5$ and for $ak = 0{\cdot}157$ and $\gamma = 0{\cdot}75$. Again we have set $U_5 = 27u_0$. When $ak = 0{\cdot}01$, the maximum pressure phase shift is significantly reduced and occurs at a lower value of c/u_0 compared with the constant z_0 values; see figure 6. The maximum is about 45° when $c = 11u_0$ compared with about 90° when $c = 16u_0$ for constant z_0. For $c < 10u_0$ the phase shift reduces slowly, whereas for $c > 12u_0$ it reduces sharply with the pressure 'cut-off' (see Elliott 1972) at about $c = 16u_0$. This value is smaller than the corresponding value of $c = 18u_0$ when z_0 is constant. For $ak = 0{\cdot}01$ and variable z_0, the results follow the observational curve of Elliott fairly closely. When $ak = 0{\cdot}157$, however, the variable z_0 results only differ slightly from those for constant z_0; compare figures 6 and 11; and the pressure 'cut-off' occurs at about $c = 18u_0$. With our chosen values of z_0 and R

[see (4.1)], this 'cut-off' lies in the range $1{\cdot}5 < U_5/c < 1{\cdot}7$ depending upon amplitude. An increase in z_0 would reduce the value of U_5/c and vice versa. Also, evidence from Townsend's (1972) table 2 for $R = 10$ and 12 suggests that for longer wavelengths (higher R) the 'cut-off' occurs at higher values of c/u_0 and thus at lower values of U_5/c. Snyder (1974) finds the 'cut-off' when $U_5/c = 1{\cdot}2$ whereas Elliott's (1972) value is $U_5/c = 2$. Elliott relates the occurrence of this 'cut-off' to the height of the critical layer compared with the wave amplitude, but we believe this to be misleading.

In figure 12 the fractional rate of energy gain per radian advance in phase, ζ, is plotted against U_5/c. Our results are for variable z_0 with $\delta = \frac{1}{4}\pi$ as in figure 11. The smaller values of ζ occur with the larger amplitude ($ak = 0{\cdot}157$) except for $c = 16u_0$. The figure shows that the onset of generation is predicted to occur when U_5/c reaches approximately 1·6, which is, of course, where the pressure phase becomes positive. Also plotted on figure 12 are the observations from three field experiments. Dobson (1971) found an energy input rate large enough to match the observed rates of wave growth measured by Snyder & Cox (1966) and Barnett & Wilkerson (1967). All subsequent observations, however, have given much lower rates. Snyder (1974) finds the energy input rate to be of the same order of magnitude as the theories of Miles and Townsend, whereas Elliott (1972) found a rate of about twice that given by linear theories. The curve based on Elliott's values bisects most of our intervals, and his observations give the best agreement with our results.

As Townsend (1972) pointed out, the critical layer is "merely an unimportant part of an equilibrium layer if turbulent stresses are included through the turbulent energy equation". Thus he was surprised that the fractional rates of energy gain per radian advance in phase he found were very similar to those of the Miles (1959) laminar critical-layer model. Further development of the Miles theory was made by Phillips (1966, § 4.3) and Miles (1967), both of whom added an extra energy input term due to the turbulent nature of the flow. Townsend's results indicate, however, that this term must be relatively small in the range $0 < c < 20u_0$, and all three predict fractional energy input rates that are similar to those found in this work when the roughness length is constant and the wave amplitude is small or large. When the roughness length varies along the wave, however, and $8u_0 < c < 12u_0$, we predict much larger fractional energy input rates when the wave amplitude is small. Whether the roughness length is constant or varying, the facts that the velocity profile $\overline{U}$ is a function of ξ as well as μ and that $c > 0$ imply that there must be a region of closed streamlines above the waves which encompasses the critical layer, as shown in figures 5 and 10. The Reynolds stresses are non-zero through the critical layer and so direct comparison with laminar critical-layer models is again difficult. They include those of Benney & Bergeron (1969) and Davis (1969), who both matched their inviscid laminar solutions across the critical layer by including the nonlinear terms rather than employing the more traditional method of including the viscous terms to give an Orr–Sommerfeld type of equation. Both these theories of the structure of closed streamlines around the critical layer have the Reynolds stresses everywhere zero.

7. Conclusions

There are two main conclusions to be drawn from the present model. The first is that with constant surface roughness, increasing wave amplitude does not produce an increased rate of fractional energy input to the waves. In fact, ζ decreases slightly as ak increases. It should be remarked, however, that for high amplitude the form drag or pressure contribution to the horizontal stress on the water surface is a significant fraction of the total. As an extreme example, the pressure contribution is more than 50 % when $c = 8u_0$ and $ak = 0{\cdot}314$. Thus the value of ζ obtained from this run is over half the maximum possible value for a given total horizontal stress on the lower surface.

The second conclusion is that if the surface roughness is allowed to vary along the wave, then at small amplitudes the values of the fractional rate of energy input are found to be up to three times the rates predicted by the linear, constant z_0, theories. The effect of varying z_0 decreases with increasing amplitude, so that when $ak = 0{\cdot}157$ the predicted fractional energy input rate is only just greater than that predicted for constant surface roughness.

Finally, it should be noted that even at the largest amplitude used, $ak = 0{\cdot}314$, the surface shear stress never fell to zero at any point along the wave.

The turbulence model and form for z_0 used in this paper are open to criticism. Refinements could be made but more detailed observations of the flow over water waves are needed as guidance. One possibility is to include streamline curvature effects by analogy with buoyancy effects in the atmosphere. These have been studied by Bradshaw (1973) and used in the work of Taylor *et al.* (1976). We feel, however, that the relative simplicity of the model used here does not invalidate the two main conclusions of this work.

The authors are very grateful to Prof. K. Hasselmann and Prof. M. S. Longuet-Higgins for several helpful discussions and wish to acknowledge the support of the Natural Environment Research Council under grant GR3/1932.

REFERENCES

BARNETT, T. P. & KENYON, K. E. 1975 *Rep. Prog. Phys.* **38**, 667.
BARNETT, T. P. & WILKERSON, J. C. 1967 *J. Mar. Res.* **25**, 292.
BENJAMIN, T. B. 1959 *J. Fluid Mech.* **6**, 161.
BENNEY, D. J. & BERGERON, R. F. 1969 *Studies in Appl. Math.* **48**, 181.
BRADSHAW, P. 1973 *AGARDOgraph*, no. 169.
BUSCH, N. E. 1973 *Workshop on Micrometeorology* (ed. Haugen). Boston: Am. Met. Soc.
CHORIN, A. J. 1967 *J. Comp. Phys.* **2**, 12.
DAVIS, R. E. 1969 *J. Fluid Mech.* **36**, 337.
DAVIS, R. E. 1972 *J. Fluid Mech.* **52**, 287.
DOBSON, F. W. 1971 *J. Fluid Mech.* **48**, 91.
ELLIOTT, J. A. 1972 *J. Fluid Mech.* **54**, 427.
HASSELMANN, K. *et al.* 1973 *Dsch. Hydro. Z. Reihe* A(8°), no. 12.
HINZE, J. O. 1959 *Turbulence*. McGraw-Hill.
KELLER, W. C. & WRIGHT, J. W. 1975 *Radio Sci.* **10**, 139.

KENDALL, J. M. 1970 *J. Fluid Mech.* **41**, 259.
LAMB, H. 1932 *Hydrodynamics*. Cambridge University Press.
LARSON, T. R. & WRIGHT, J. W. 1975 *J. Fluid Mech.* **70**, 417.
LONG, R. B. 1971 Ph.D. thesis, University of Miami, Florida.
LONGUET-HIGGINS, M. S. 1969*a* *Proc. Roy. Soc.* A **311**, 371.
LONGUET-HIGGINS, M. S. 1969*b* *Phys. Fluids*, **12**, 737.
MILES, J. W. 1957 *J. Fluid Mech.* **3**, 185.
MILES, J. W. 1959 *J. Fluid Mech.* **6**, 568.
MILES, J. W. 1967 *J. Fluid Mech.* **30**, 163.
PHILLIPS, O. M. 1966 *The Dynamics of the Upper Ocean*. Cambridge University Press.
REYNOLDS, W. C. & HUSSAIN, A. K. M. F. 1972 *J. Fluid Mech.* **54**, 263.
SHEMDIN, O. H. 1969 *Coastal Engng Lab., Univ. Florida, Tech. Rep.* no. 4.
SHEMDIN, O. H. & LAI, R. J. 1973 *Coastal Engng Lab., Univ. Florida, Tech. Rep.* no. 18.
SNYDER, R. L. 1974 *J. Mar. Res.* **32**, 497.
SNYDER, R. L. & COX, C. S. 1966 *J. Mar. Res.* **24**, 141.
TAYLOR, P. A., GENT, P. R. & KEEN, J. M. 1976 *Geophys. J. Roy. Astr. Soc.* **44**, 177.
TOWNSEND, A. A. 1972 *J. Fluid Mech.* **55**, 719.